DOI: 10.11916/j.issn.1005-9113.2018005

Effect of Thermal Regeneration on the Breakthrough Performance of Ceramsite Saturated with Methylene Blue

Tianpeng Li[1] and Ting Li[2]*

(1. College of City and Architecture Engineering, Zaozhuang University, Zaozhuang 277160, China;

2. Zaozhuang Yuanheng Machinery Manufacturing Co., Ltd., Zaozhuang 277000, China)

Abstract: The regeneration of a spent packing is crucial with respect to the development of circular economy and abstemious society. Thus, the effects of regeneration temperature, resistant time, heating rate, and regeneration cycle on the breakthrough performance of methylene blue (MB) dye-exhausted ceramsite in a two-stage fixed-bed column were studied in this work. Results illustrate that the ceramsite exhibited excellent potential regeneration properties under the following optimal regeneration conditions: treatment temperature was 600 ℃, resistant time was 15 min, heating rate was 20 ℃/min, regeneration cycle was over 9 cycles, and the breakthrough time, saturation time, regeneration efficiency (RE), and regeneration loss rate (RLR) were 540 min, 1020 min, 64.61%, and 17.73%, respectively. The RE declined by 35.14% in over 1 cycle, while the RLR increased by 3.15 times in over 9 cycles. Besides, Thomas model was suitable to describe the two-stage fixed-bed column adsorption and thermal regeneration process with R^2 = 0.978. In conclusion, a thorough understanding of the regeneration behavior of the two-stage fixed-bed column packed with ceramsite provides reference to obtain an effective and feasible regeneration approach, and it is beneficial for further application in water treatment.

Keywords: ceramsite; thermal regeneration; two-stage fixed-bed column; breakthrough performance; Thomas model

CLC number: X7 **Document code**: A **Article ID:**

1 Introduction

With the economic development and the strictness of environmental standards, the removal of dye prior to its discharge into the environment should be considered because of the detriment of discharged color to the receiving water bodies and the impact of their coloration on the photosynthesis of aquatic plants[1-3]. Colored effluents can be treated by adsorption-based process since it is much simpler to maintain, less energy-intensive, more efficient, and has lower initial costs than other available physico-chemical or biochemical techniques. Among all these methods,

Received 2018-11-27.
Sponsored by the Natural Science Foundation Training Project of Shandong Province, China (Project No. ZR2018PEE026), the Science and Technology Planning Project of Zaozhuang City, Shandong Province, China (Project No. 2018GX12), the Project of Science Research Foundation of Zaozhuang University, China (Project No. 2017ZX16), and the Doctoral Scientific Research Foundation of Zaozhuang University, China (Project No. 2017BS01).
Corresponding author. E-mail address: tianpeng985@126.com.

adsorption is an effective and mature method to treat industrial wastewater[4-6].

To implement the adsorption method, fixed-bed column has received increasingly more attention to obtain basic engineering data required to realize industrial scale applications[7-9]. Compared with batch adsorption method, the column experiment is becoming more and more popular due to its prominent advantages, such as simple mode operation, high removal efficiency, and accurate prediction of the experimental results. Furthermore, the fixed-bed column adsorption is closer to the industrial application than laboratory experiments.

Several kinds of packing, such as activated carbon (AC)[10], pyroxene nanoparticles embedded on Diatomite[11], natural iron mineral-quartz sand[12], and chitosan coated glass beads[13], have been extensively studied in fixed-bed columns. However, the high cost and complex fabrication process of these fillings limit their applicability, whereas materials obtained from wastes appear as interesting and cheap alternatives with operational simplicity, cost effectiveness, and regenerative capability[14].

In the last few years, with unique surface morphology, crystal structure, and multi-functional properties, ceramsite, as a kind of promising mesoporous material, has been widely studied and applied[15-17]. Since ceramsite can be obtained from solid wastes without adding any non-renewable natural resources, it has been adopted to treat wastewater, such as removal of heavy metal from stormwater runoff[18], removal of anthracenemethanol from soil[19], and immobilization of phosphorus in constructed wetlands[20]. As is known, when ceramsite reaches its saturation limit within the application time, it fails to adsorb the targeted pollutants, leading to the dramatical decrease of its removal performance. In general, the exhausted materials are mostly discarded in the landfills. However, to achieve a more sustainable development and prevent environmental contamination, it is indispensable that the deactivated ceramsite should be regenerated to meet the removal requirement[21]. It is better to recover the removal performance of exhausted materials than to discard them carelessly[22]. Additionally, some studies have demonstrated that regeneration and management of spent materials play crucial roles in the operation of wastewater treatment, which is critical to the sustainability of the adsorption-based process[23-24]. This has become an important issue from both academic and industrial perspectives, as well as from an economic point of view.

Many regeneration technologies have been developed, including ultrasound-assisted regeneration[25], advanced oxidation technology (AOT)[26], and pressure swing adsorption (PSA)[27], which, however, have shortcomings. For example, PSA is energy-consuming and has high installation costs. AOT costs a lot of water and chemical reactants, leading to significant economic and environmental impacts. Ultrasound-assisted regeneration also has several disadvantages, such as long regeneration period,

follow-up processing, and easily causing secondary pollution. As a conventional regeneration method, the principle of thermal decomposition is that the essential energy is provided to heat the spent materials and remove the retained adsorbate[28]. Despite the appearance of many new technologies in this field, thermal decomposition is still an effective and easy method for regeneration[29-31].

Hence, an experimental investigation on the thermal regeneration of MB dye-spent ceramsite in a two-stage fixed-bed column was carried out. Firstly, a two-stage fixed-bed column adsorption and thermal regeneration process was designed based on our preceding studies. Secondly, effects of regeneration temperature, resistant time, heating rate, and regeneration cycle on the breakthrough curves (BTCs) of MB dye for regenerated ceramsite were analyzed. Finally, the impact mechanism of thermal regeneration on the two-stage fixed-bed column packed with ceramsite was discussed.

2 Experiment and Methods

2.1 Materials and Reagents

Without adding any non-renewable natural resources, the lab-made ceramsite was prepared by a high-temperature sintering process in this work, which was obtained from solid wastes (including dewatered sewage sludge, coal fly ash, and river sediment). The methods of preparation processes, high-temperature control curve of sintering process, characterization techniques, and the results of physical-chemical properties and heavy metal leaching toxicities of ceramsite were illustrated in our published paper[32]. In brief, the physical properties of breaking and wear rate, solubility in hydrochloric acid, silt carrying capacity, void fraction, BET specific surface area, and piled density of ceramsite are 0.2%, 0.01%, 0.2%, 71.1%, 0.75×10^4 cm^2/g, and 0.95 g/cm^3, respectively, which were in accordance with the industrial standard (CJ/T 299-2008) and the national standard (GB5085.3-2007). The results demonstrated that the lab-made ceramsite is safe and reliable, reflecting a good application future in the field of wastewater treatment. The ceramsite was crushed down and sieved to a desired diameter before application. It was then cleaned multiple times with deionzied water to remove the impurities in the inner pores and was dried at 60 $^{\circ}C$ for over 10 h.

MB dye, received from Sinopharm Chemical Reagent Co., Ltd., China, is a phenothiazine cation ($C_{16}H_{18}N_3SCl$; molecular weight 319.86) according to analytical grade. It was employed in this study as a model molecular for organic pollutant in general and basic dye in particular, which was used as received without further purification. The stock solution (500 mg/L) was prepared by accurately dissolving the weighed quantity of the MB dye in deionized water. The initial concentration of the MB dye was prepared thereafter by diluting the abovementioned stock solution, and the deionized water was employed in all experiments.

2.2 Column Adsorption and Thermal Regeneration Process

The schematic diagram of the two-stage fixed-bed

column adsorption and thermal regeneration process used in this experiment is shown in Fig.1. For all the experiments, the initial experimental conditions were maintained at constant values, including initial pH (3.0), initial concentration of MB dye (5 mg/L), inlet flow rate (33 mL/min), and particle diameter of ceramsite (0.5±0.2 mm). All the experiments were investigated at room temperature and atmospheric pressure. The experimental process includes two following parts:

First, the two-stage fixed-bed column consists of two cleaned cylindrical glass tubes in parallel, whose internal diameter, column height, and valid volume are 7.5 cm, 50 cm, and 2.2×10^3 cm^3, respectively. A filter cloth was placed at the top and bottom of each tube to avoid the penetration of packing, and a certain amount of ceramsite was packed into the tubes. Influent was fed into the column from the bottom of one tube and effluent was discharged from the top of the other tube. At different time intervals, the effluents were collected. Then, the absorbance of the MB dye was measured at its maximum wavelength of 664 nm by UV-Vis spectrophotometer (UV-5500, Shanghai Metash Instruments Co., Ltd., China).

Second, the exhausted ceramsite was collected in quartz crucibles and placed into a furnace (SX2-10-17, Shanghai Yifeng Electric Furnace Co., Ltd., China). After preheated at 125 °C for 20 min, the exhausted ceramsite was heated in air atmosphere according to the designed regeneration temperature and resistant time, and then was naturally cooled down to room temperature. Subsequently, the regenerated ceramsite was cleaned for several times with deionzied water to remove any impurities and was dried for about 10 h at 60 °C. Finally, the regenerated ceramsite was put into the columns, and the column experiment was thus carried out according to the initial part.

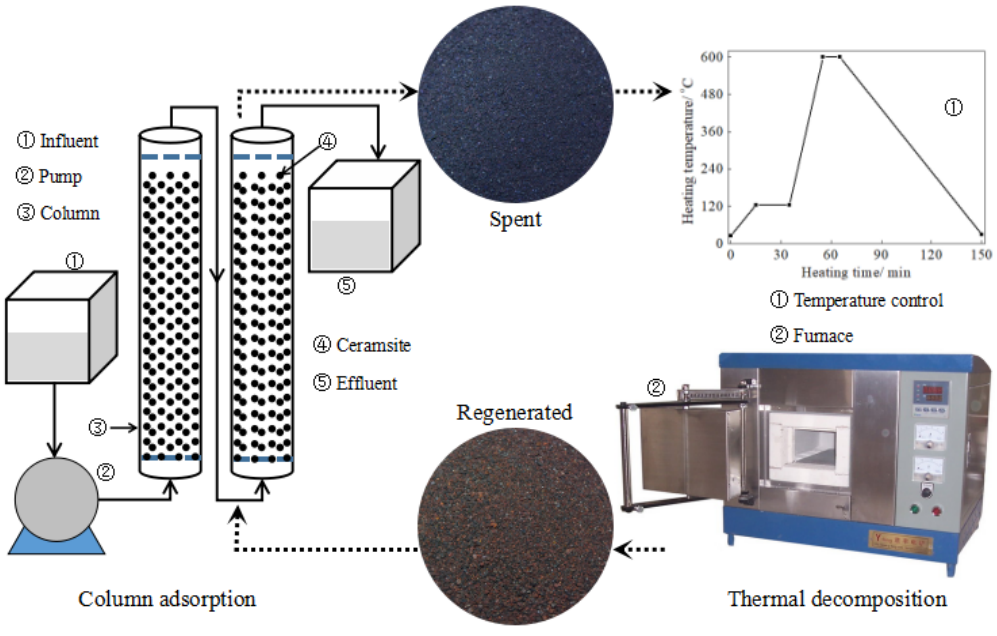

Fig.1 Schematic diagram of two-stage fixed-bed column adsorption and thermal regeneration process

2.3 Analysis

BTCs were received by plotting C_t/C_0 against t, where C_t (mg/L), C_0 (mg/L), and t (min) are the effluent concentration, initial concentration, and operating time. The point where the C_t reaches about 5% of the C_0 is the breakthrough point (C_t = 5% C_0), and the corresponding time is breakthrough time. The point where the C_t reaches 90% of the C_0 is the exhaustion point (C_t = 90% C_0), and the corresponding time is saturation time.

The surface morphology of the samples was observed by SEM-EDS (scanning electron microscope-energy dispersive spectrometer, JSM7800F, JEOL, Japan) with an accelerating voltage of 13 kV. Before measurement, the surface of the samples was sputtered with gold layer to improve the quality of the images. The BET specific surface area (S_{BET}), pore size distribution, and the values for the average pore size were calculated from N_2 adsorption and desorption measurements by using a fully automatic specific and micro pore size analyzer (ASAP 2020HD88, Micromeritics, USA).

Thomas model assumes the second-order reversible reaction kinetics and the Langmuir isotherm, which is one of the most generally and widely used models to describe the performance theory of the sorption process in fixed-bed columns. The linearized expression of the model is given as follows:

$$\ln\left(\frac{C_t}{C_0 - C_t}\right) = K_{TH}C_0 t - \frac{K_{TH}q_i m}{V} \quad (1)$$

where C_0 is the initial concentration (mg/L), C_t is the effluent concentration (mg/L), K_{TH} is the rate constant (mL/min/mg), q_i is the maximum adsorption capacity in a given ith re-use cycle (mg/g), m is the amount of adsorbent in the fixed-bed column (g), and v is the volumetric flow rate (mL/min). The parameters K_{TH}, R^2, and q_i can be calculated from the linear plot of $ln[Ct/(C_0\text{-}C_t)]$ against t.

The standard equation of regeneration efficiency (RE) (%) is defined as the comparison between the adsorption capacities of the regenerated ceramsite against the original ceramsite[33]. The RE and RLR (%) can be calculated by Eq. (2) and Eq. (3), respectively.

$$\mathrm{RE} = \frac{Q_i}{Q_0} \times 100\% \quad (2)$$

where Q_0 and Q_i are the initial adsorption capacity of ceramsite and the adsorption capacity of the regenerated ceramsite in a given ith re-use cycle (mg/g).

$$\mathrm{RLR} = \frac{m_0 - m_i}{m_0} \times 100\% \quad (3)$$

where m_0 is the initial mass of ceramsite (kg), and m_i is the mass of the regenerated ceramsite in a given ith re-use cycle (kg).

3 Results and Discussion

3.1 Effect of Regeneration Temperature

The effect of regeneration temperature on the shape of BTCs and dynamic behavior was investigated at four different regeneration temperatures (300, 450, 600, and 750 °C). It can be seen from Fig.2(a) that with the increase of regeneration temperature, both breakthrough and saturation times gradually shifted to the right so that the shape of BTC became more and

more smooth. At lower regeneration temperatures, the breakthrough and exhaustion both occurred faster. Within the investigated regeneration temperatures, the breakthrough time increased significantly, e.g., 480 min for 300 ℃, 520 min for 450 ℃, 680 min for 600 ℃, and 700 min for 750 ℃. A similar trend was also found for saturation time (Fig.2(a)).

As shown in Table 1, regeneration temperature had much greater influence on RE, but its effect on RLR was relatively low. The value of RE was 99.75% at 600 ℃, which was 33.7% higher than that of 300 ℃. One possible reason for this tendency is that a higher regeneration temperature accelerates energy transference and reduces the residence time of the adsorbates[34], resulting in a much thorough decomposition of MB dye, which moderately renders BTCs smooth. The value of RLR also increased with the increase of regeneration temperature. The reasons might be that at a higher regeneration temperature (750 ℃), ceramsite is more prone to conduct cracking reaction and its particle becomes smaller. Therefore, the ceramsite is more easily to be lost, especially in the process of washing[35].

Considering that the treatment temperature of 600 ℃ offered an optimum BTC, especially for the values of RE and RLR, the subsequent experiments were carried out at 600 ℃.

Table 1 Results of fitting parameters of Thomas model, RE, and RLR under different experiment conditions

Regeneration conditions		Thomas model			RE (%)	RLR (%)
		$k_{TH}\times10^{-3}$ (mL/min/mg)	q_i (mg/g)	R^2		
Regeneration temperature (°C)	300	1.52	26.13	0.947	66.05	4.57
	450	1.52	27.66	0.935	69.92	4.88
	600	1.44	39.46	0.978	99.75	5.62
	750	1.56	38.75	0.985	97.95	6.63
Resistant time (min)	5	1.54	31.22	0.972	78.92	5.14
	15	1.44	39.46	0.978	99.75	5.62
	25	1.7	37.55	0.974	94.92	6.15
	35	1.64	38.12	0.977	96.36	6.56
Heating rate (°C/min)	5	1.46	39.53	0.965	99.92	6.12
	10	1.44	39.54	0.974	99.95	6.05
	20	1.44	39.46	0.978	99.75	5.62
	30	1.6	32.72	0.966	82.71	5.31
Regeneration cycle	1	1.44	39.46	0.978	99.75	5.62
	3	1.52	36.91	0.974	93.3	7.49
	5	1.5	33.84	0.953	85.54	10.05
	7	1.52	29.21	0.963	73.84	13.23
	9	1.68	25.56	0.956	64.61	17.73

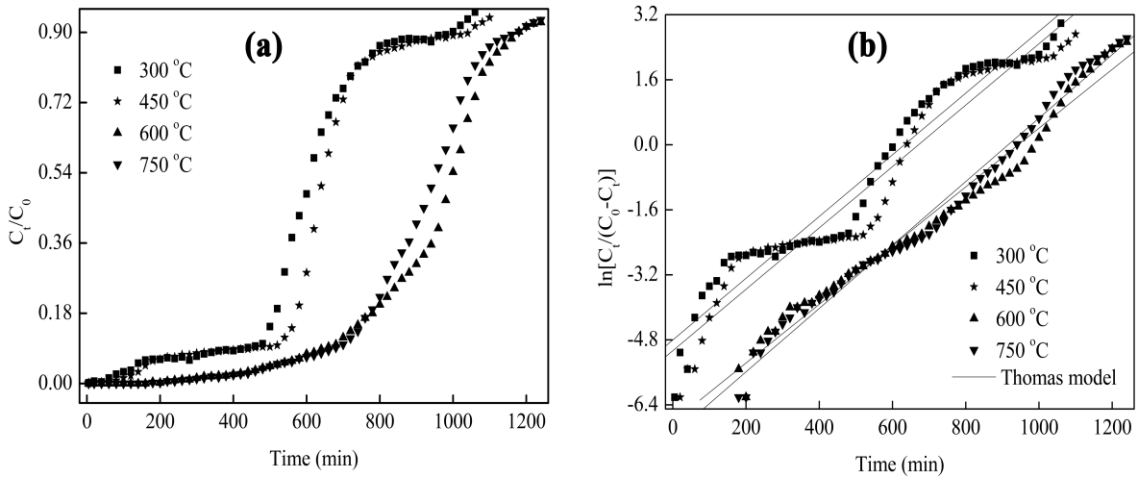

Fig.2 (a) Effect of regeneration temperature on BTCs for MB dye removed from aqueous solution (experiment conditions: resistant time was 15 min and heating rate was 20 °C/min); (b) Linear fitting of Thomas model for MB dye

3.2 Effect of Resistant Time

The effect of resistant time (in the range of 5~35 min) on the MB dye removal in the two-stage fixed-bed column packed with regenerated ceramsite was revealed by BTCs, and the results are presented in Fig.3 and Table 1. Fig.3(a) indicates that BTC became more and more gentle with the increase of resistant time. The breakthrough time increased from 580 to 720 min when the resistant time increased from 5 to 25 min. However, it had no further increase when the resistant time continued increasing from 25 to 35 min. The saturation time showed a similar tendency during the whole investigated resistant time.

As illustrated in Table 1, with the prolonged resistant time, the value of RLR was increased gradually (< 6.6%) with no significance. In addition, the value of RE was increased by 20.83% when the resistant time was 15 min, compared with the resistant time at 5 min. By contrast, as the resistant time continued to increase from 15 to 35 min, RE had no obvious improvement, which is around 95%. This can be interpreted by the fact that shorter resistant time makes it more uneven for heat to transfer in the spent ceramsite, especially for the inner porous structure of the ceramsite, which eventually results in the suppression of the decomposition of MB dye molecule[36]. On the other hand, ceramsite is a mesoporous material with irregular shape and rough surface, so when it is heated for a longer resistant time, more complex physical, chemical, or physicochemical reaction occurs during the thermal regeneration, leading to the partial removal of the surface functional groups of ceramsite, which in turn changes the pore structure[37-38]. Thus, taking into account of RE and RLR, the resistant time of 15 min was chosen as the optimal condition to study the effect of other factors on the removal performance of ceramsite in the two-stage fixed-bed column.

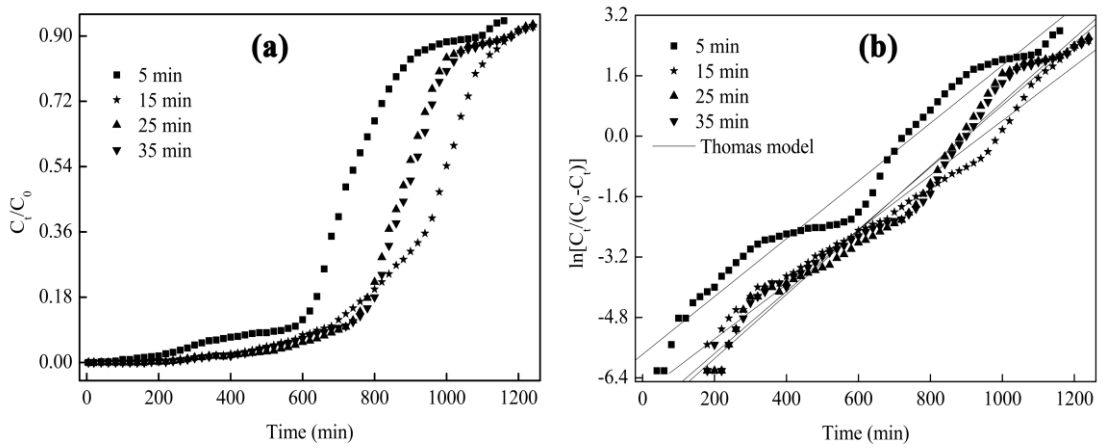

Fig.3 (a) Effect of resistant time on BTCs for MB dye removed from aqueous solution (experiment conditions: regeneration temperature was 600 °C and heating rate was 20 °C/min); (b) Linear fitting of Thomas model for MB dye

3.3 Effect of Heating Rate

The effect of different heating rates (5, 10, 20, and 30 °C/min) on the breakthrough point was analyzed. It was found that the breakthrough point gradually occurred earlier with the increase of heating rate (Fig.4(a)). As the heating rate was changed from 5 to 30 °C/min, the breakthrough time decreased from 740 to 620 min. Meanwhile, the saturation time decreased slightly.

It is noteworthy that with the increase of the heating rate from 5 to 20 °C/min, the value of RE was found to be unchanged at around 99.9%. On the contrary, the value of RE exhibited a significant reduction when the heating rate changed from 20 to 30 °C/min, declining by about 10%. This may be attributed to the fact that higher heating rate prevents MB dye molecule from complete decomposition, leading to a lower value of RE. Besides, the value of RLR showed a downward trend during the whole experiment, but it had a negligible change because of the elimination of residual moisture as well as the pyrolysis and volatilisation of organic compounds accumulated in the ceramsite porosity[39]. As discussed above, it was suggested that the preferable heating rate is 20 °C/min for recovering adsorption capacity of ceramsite in the column adsorption-thermal regeneration process.

3.4 Effect of Regeneration Cycle

With the following preferable regeneration conditions: temperature was 600 °C, resistant time was 15 min, and heating rate was 20 °C/min, the effects of regeneration cycles on the thermal regeneration characteristics of ceramsite saturated with MB dye in the two-stage fixed-bed column were investigated by setting the variable to 1, 3, 5, 7, and 9 cycles. Results showed that the slope of BTC increased with the change of regeneration cycle, and both breakthrough and saturation times decreased simultaneously (Fig.5(a)). Furthermore, when the regeneration cycle was at 1, 3, 5, 7, and 9 cycles, the breakthrough time

was 680, 680, 660, 600, and 540 min, respectively. Similarly, an increase in regeneration occurred from the first cycle to the last cycle, which brought to the decrease of saturation time from 1180 to 1020 min. These results suggest a negative relationship between regeneration cycles and removal capacity of the two-stage fixed-bed column adsorption, which were consistent with the previous reports[40-41].

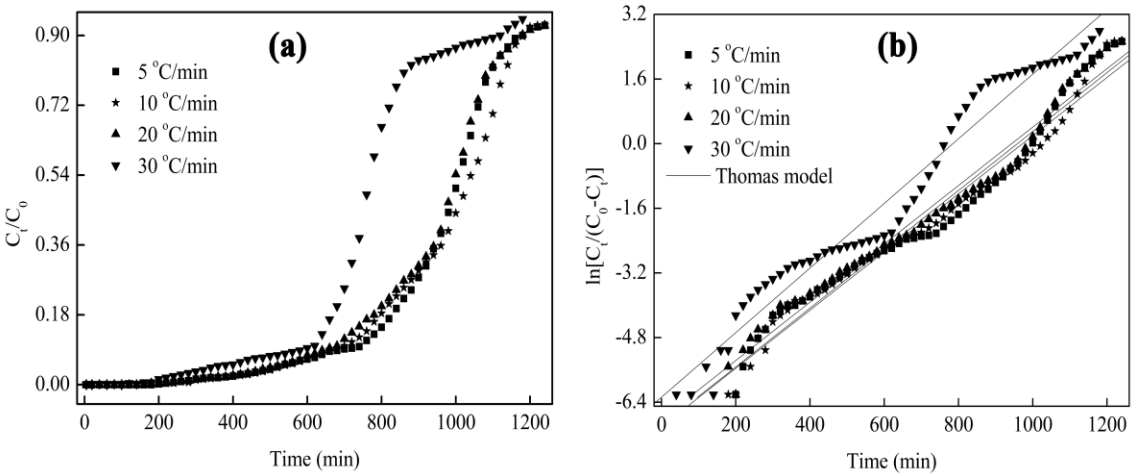

Fig.4 (a) Effect of heating rate on BTCs for MB dye removed from aqueous solution (experiment conditions: regeneration temperature was 600 °C and resistant time was 15 min); (b) Linear fitting of Thomas model for MB dye

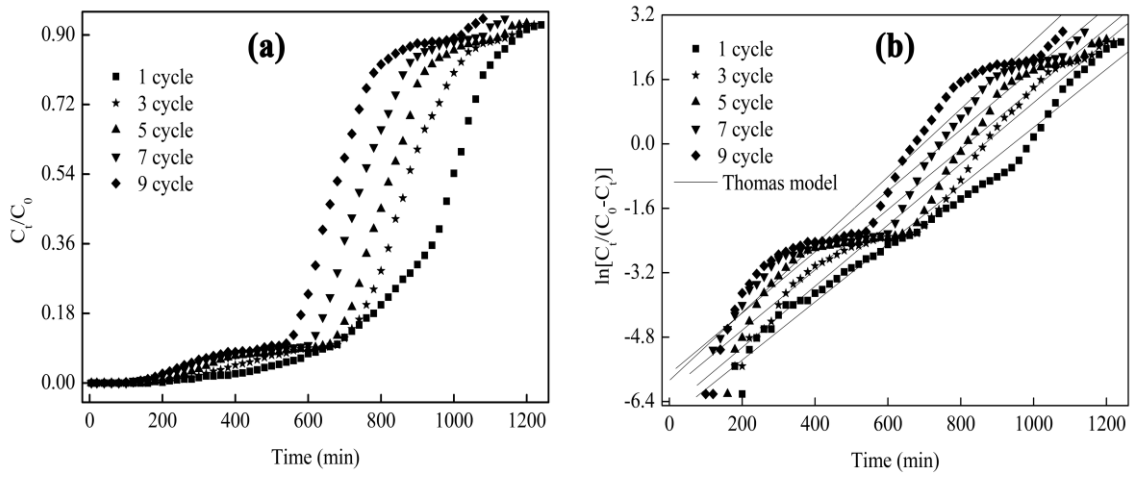

Fig.5 (a) Effect of regeneration cycle on BTCs for MB dye removed from aqueous solution (experiment conditions: regeneration temperature was 600 °C, resistant time was 15 min, and heating rate was 20 °C/min); (b) Linear fitting of Thomas model for MB dye

As is shown in Table 1, the RLR value raised along with the increase of regeneration cycle. The value of RLR was 17.73% after 9 cycles, which was lower than that of activated carbon (> 20%)[42]. The major reason is that the physical and chemical properties of ceramsite are subjected to extreme damage after repeated heating, cooling, and washing, which finally leads to more and more resistance towards the heat treatment[43].

Compared with other factors, the RE of the two-stage fixed-bed column adsorption and thermal regeneration process is largely affected by regeneration cycle. The value of RE decreased from 99.75% to 64.61% (decreased by 35.14%) with the regeneration

cycle increasing from 1 to 9 cycles. It might be attributed to the facts that (I) the SEM photos showed the surface of the ceramsite turned from smooth into rough, generating more and more impurities as the regeneration cycle increased (Figs.6(a-c)). The EDS spectra showed that the content (wt%) of non-metallic elements, such as C and O, changed dramatically with the increase of regeneration cycle, resulting in the total decrease of the active sites on the surface of ceramsite. (II) As illustrated in Table 2, the value of S_{BET} was 0.15 m^2/g in over 7 cycles, which was 76.19% lower than that of the original cycle. The value of the total pore volume decreased visibly with the increase of regeneration cycle. On the contrary, the value of the average pore diameter increased significantly in over 7 cycles, increased by 2.78 times compared with the original cycle.

Table 2 Textural properties from N_2 adsorption-desorption isotherms of regenerated ceramsite in over 3, 5, and 7 cycles

Cycles	S_{BET} (m^2/g)	Total pore volume (m^3/g)	Average pore diameter (nm)
Original	0.63	0.003	16.97
Cycle 3	0.22	0.0019	35.92
Cycle 5	0.19	0.0017	36.35
Cycle 7	0.15	0.0017	47.21

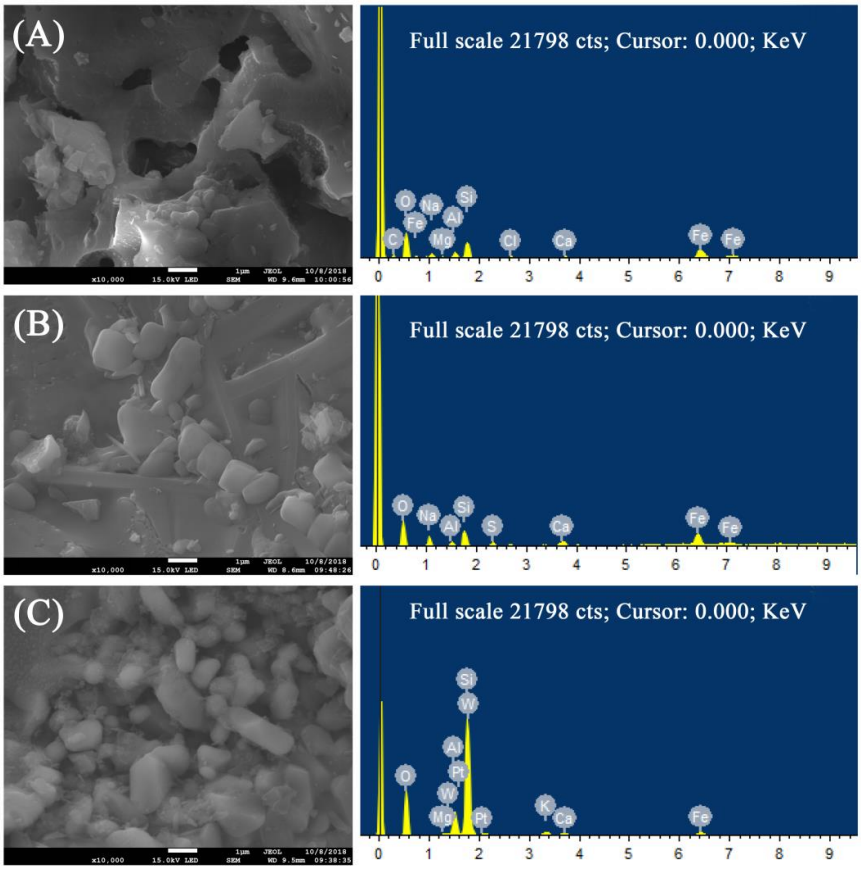

Fig.6 SEM images and EDS spectra of the regenerated ceramsite in over 3, 5, and 7 cycles

3.5 Modeling Analysis

To better evaluate the regeneration performance of the two-stage fixed-bed column packed with regenerated ceramsite, the Thomas model was employed to fit the experimental data of Fig.2(a), Fig.3(a), Fig.4(a), and Fig.5(a). The model parameters of K_{TH} and q_i for MB dye and R^2 were received using linear regression analysis according to Eq. (1), and the results are presented in Fig.2(b), Fig.3(b), Fig.4(b), Fig.5(b), and Table 1. It was noticed that the regeneration cycle exerted the greatest influence on the linear relationship between $\ln[C_t/(C_0-C_t)]$ and the operating time, followed by the regeneration temperature, while the influences of heating rate and resistant time were the slightest. With the preferable regeneration experiment conditions, i.e., regeneration temperature was 600 ℃, resistant time was 15 min, heating rate was 20 ℃/min, and regeneration cycle was over 1 cycle, the Thomas model was successfully used for predicting the BTC for MB dye removed by the two-stage fixed-bed column packed with regenerated ceramsite, which showed the higher value of R^2 of about 0.98.

Fig.5(b) and Table 1 illustrated that with increasing regeneration cycle, the value of K_{TH} increased a little. The value of K_{TH} increased from 1.44 to 1.68×10^{-3} mL/min/mg with the regeneration cycle increasing from 1 to 9 cycles, suggesting that the molecular transfer rate of MB dye from the liquid phase to the solid phase became faster as the repeat use time increased. It was noted that the value of q_i decreased obviously when regeneration cycle increased from 1 to 9. As the regeneration proceeded to 9 cycles, the q_i of MB dye with ceramsite decreased from 39.56 to 25.56 mg/g, which was 35.23% lower than that of the first cycle, suggesting that regeneration cycle greatly impacts the adsorption capacity of ceramsite. This can be explained by the fact that adsorption sites of caremsite were deactivated or disintegrated after a certain number of column adsorption-thermal regeneration process[44]. In addition, the value of R^2 decreased from 0.978 to 0.956 with the regeneration increased from 1 to 9 cycles, indicating that the fewer the regeneration time is, the more adequate the Thomas model fits the experiment data.

4 Conclusions

Two-stage fixed-bed column adsorption and thermal regeneration process was conducted to investigate the effect of thermal regeneration on ceramsite saturated with MB dye in aqueous solution. The theoretical BTC agreed with the experimental data very well under the preferable regeneration experimental conditions. Both breakthrough and saturation times were shifted from left to right gradually with the increase of regeneration temperature, resistant time, heating rate, and regeneration cycle. Thomas model showed a good agreement with the BTCs for MB dye (R^2 = 0.978), which can be applied for the prediction of the two-stage fixed-bed column adsorption behaviours. Compared with the first cycle, the breakthrough and saturation times were shortened by 140 and 160 min after the ninth cycle. Meanwhile,

within the investigated cycles of regeneration, the values of q_i and RE were more than 25.56 mg/g and 64.61% respectively, and the value of RLR was always lower than 17.73%, indicating that ceramsite has a strong potential regeneration capacity, which makes it promising for water treatment in the future.

In conclusion, thermal regeneration is a feasible approach for recovering the adsorption ability of exhausted ceramsite. The two-stage fixed-bed column packed with ceramsite has great value for study and application purposes.

References

[1] Rosales E, Anasie D, Pazos M, et al. Kaolinite adsorption-regeneration system for dyestuff treatment by Fenton based processes. Science of The Total Environment, 2018, 622-623: 556-562. DOI: 10.1016/j.scitotenv.2017.11.301.

[2] Khatri M, Ahmed F, Shaikh I, et al. Dyeing and characterization of regenerated cellulose nanofibers with vat dyes. Carbohydrate Polymers, 2017, 174: 443-449. DOI: 10.1016/j.carbpol.2017.06.125.

[3] Vieira M L G, Esquerdo V M, Nobre L R, et al. Glass beads coated with chitosan for the food azo dyes adsorption in a fixed bed column. Journal of Industrial and Engineering Chemistry, 2014, 20(5): 3387-3393. DOI: 10.1016/j.jiec.2013.12.024.

[4] Li Y J, Hu X J, Liu X L, et al. Adsorption behavior of phenol by reversible surfactant-modified montmorillonite: Mechanism, thermodynamics, and regeneration. Chemical Engineering Journal, 2018, 334: 1214-1221. DOI: 10.1016/j.cej.2017.09.140.

[5] Oyarzun D I, Hemmatifar A, Palko J W, et al. Adsorption and capacitive regeneration of nitrate using inverted capacitive deionization with surfactant functionalized carbon electrodes. Separation and Purification Technology, 2018, 194: 410-415. DOI: 10.1016/j.seppur.2017.11.027.

[6] Ren J, Li N, Li L, et al. Granulation and ferric oxides loading enable biochar derived from cotton stalk to remove phosphate from water. Bioresource Technology, 2015, 178: 119-125. DOI: 10.1016/j.biortech.2014.09.071.

[7] Gouran-Orimi R, Mirzayi B, Nematollahzadeh A, et al. Competitive adsorption of nitrate in fixed-bed column packed with bio-inspired polydopamine coated zeolite. Journal of Environmental Chemical Engineering, 2018, 6(2): 2232-2240. DOI: 10.1016/j.jece.2018.01.049.

[8] Darweesh T M, Ahmed M J. Adsorption of ciprofloxacin and norfloxacin from aqueous solution onto granular activated carbon in fixed bed column. Ecotoxicology and Environmental Safety, 2017, 138: 139-145. DOI: 10.1016/j.ecoenv.2016.12.032.

[9] Gong J L, Zhang Y L, Jiang Y, et al. Continuous adsorption of Pb(II) and methylene blue by engineered graphite oxide coated sand in fixed-bed column. Applied Surface Science, 2015, 330: 148-157. DOI: 10.1016/j.apsusc.2014.11.068.

[10] Franco M A E D, Carvalho C B D, Bonetto M M, et al. Removal of amoxicillin from water by adsorption onto activated carbon in batch process and fixed bed column: Kinetics, isotherms, experimental design and breakthrough curves modelling. Journal of Cleaner Production, 2017, 161: 947-956. DOI: 10.1016/j.jclepro.2017.05.197.

[11] Hethnawi A, Nassar N N, Manasrah A D, et al. Polyethylenimine-functionalized pyroxene nanoparticles embedded on Diatomite for adsorptive removal of dye from textile wastewater in a fixed-bed column. Chemical Engineering Journal, 2017, 320: 389-404. DOI: 10.1016/j.cej.2017.03.057.

[12] Guo H M, Stüben D, Berner Z. Arsenic removal from water using natural iron mineral-quartz sand columns. Science of The Total Environment, 2007, 377(2-3): 142-151. DOI: 10.1016/j.scitotenv.2007.02.001.

[13] Vieira M L G, Martinez M S, Santos G B, et al. Azo dyes adsorption in fixed bed column packed with different deacetylation degrees chitosan coated glass beads. Journal of Environmental Chemical Engineering, 2018, 6(2): 3233-3241. DOI: 10.1016/j.jece.2018.04.059.

[14] Ye Y Y, Yang J, Jiang W, et al. Fluoride removal from water using a magnesia-pullulan composite in a continuous fixed-bed column. Journal of Environmental Management, 2018, 206: 929-937. DOI: 10.1016/j.jenvman.2017.11.081.

[15] Zhao D, Gao Y N, Nie S, et al. Self-assembly of honeycomb-like calcium-aluminum-silicate-hydrate (C-A-S-H) on ceramsite sand and its application in photocatalysis. Chemical Engineering Journal, 2018, 344: 583-593. DOI: 10.1016/j.cej.2018.03.074.

[16] Jing Q X, Wang Y Y, Chai L Y, et al. Adsorption of copper ions on porous ceramsite prepared by diatomite and tungsten residue. Transactions of Nonferrous Metals Society of China, 2018, 28(5): 1053-1060. DOI: 10.1016/S1003-6326(18)64731-4.

[17] Li T P, Sun T T, Aftab T B, et al. Comparative study between ceramsite media and quartz sand for the removal of methylene blue dye from aqueous solution in fxed-bed columns.

Desalination and Water Treatment, 2019, 139: 53-63. DOI: 10.5004/dwt.2019.23460.

[18] Wang J L, Zhao Y L, Zhang P P, et al. Adsorption characteristics of a novel ceramsite for heavy metal removal from stormwater runoff. Chinese Journal of Chemical Engineering, 2018, 26(1): 96-103. DOI: 10.1016/j.cjche.2017.04.011.

[19] Wang M, Zhang G L, Pang T, et al. Removal of anthracenemethanol from soil through a magnetic system assisted by ceramsite coated with nanoflower-structured carbon and preparation for its engineering application. Chemical Engineering Journal, 2017, 328: 748-758. DOI: 10.1016/j.cej.2017.07.074.

[20] Cheng G, Li Q H, Su Z, et al. Preparation, optimization, and application of sustainable ceramsite substrate from coal fly ash/waterworks sludge/oyster shell for phosphorus immobilization in constructed wetlands. Journal of Cleaner Production, 2018, 175: 572-581. DOI: 10.1016/j.jclepro.2017.12.102.

[21] Liu C, Sun Y K, Wang D Y, et al. Performance and mechanism of low-frequency ultrasound to regenerate the biological activated carbon. Ultrasonics Sonochemistry, 2017, 34: 142-153. DOI: 10.1016/j.ultsonch.2016.05.036.

[22] Sun Y L, Zhang B, Zheng T, et al. Regeneration of activated carbon saturated with chloramphenicol by microwave and ultraviolet irradiation. Chemical Engineering Journal, 2017, 320: 264-270. DOI: 10.1016/j.cej.2017.03.007.

[23] Ateia M, Ceccato M, Budi A, et al. Ozone-assisted regeneration of magnetic carbon nanotubes for removing organic water pollutants. Chemical Engineering Journal, 2018, 335: 384-391. DOI: 10.1016/j.cej.2017.10.166.

[24] Singh R, Gbordzoe E. Modeling FCC spent catalyst regeneration with computational fluid dynamics. Powder Technology, 2017, 316: 560-568. DOI: 10.1016/j.powtec.2016.10.058.

[25] Yao Y. Enhancement of mass transfer by ultrasound: Application to adsorbent regeneration and food drying/dehydration. Ultrasonics Sonochemistry, 2016, 31: 512-531. DOI: 10.1016/j.ultsonch.2016.01.039.

[26] Tang S F, Yuan D L, Li N, et al. Hydrogen peroxide generation during regeneration of granular activated carbon by bipolar pulse dielectric barrier discharge plasma. Journal of the Taiwan Institute of Chemical Engineers, 2017, 78: 178-184. DOI: 10.1016/j.jtice.2017.05.025.

[27] Farooq M, Almustapha M N, Imran M, et al. In-situ regeneration of activated carbon with electric potential swing desorption (EPSD) for the H_2S removal from biogas. Bioresource Technology, 2018, 249: 125-131. DOI: 10.1016/j.biortech.2017.09.198.

[28] Salvador F, Martin-Sanchez N, Sanchez-Hernandez R, et al. Regeneration of carbonaceous adsorbents. Part I: Thermal Regeneration. Microporous and Mesoporous Materials, 2015, 202: 259-276. DOI: 10.1016/j.micromeso.2014.02.045.

[29] Cazetta A L, Junior O P, Vargas A M M, et al. Thermal regeneration study of high surface area activated carbon obtained from coconut shell: Characterization and application of response surface methodology. Journal of Analytical and Applied Pyrolysis, 2013, 101: 53-60. DOI: 10.1016/j.jaap.2013.02.013.

[30] Duan X H, Srinivasakannan C, Liang J S. Process optimization of thermal regeneration of spent coal based activated carbon using steam and application to methylene blue dye adsorption. Journal of the Taiwan Institute of Chemical Engineers, 2014, 45(4): 1618-1627. DOI: 10.1016/j.jtice.2013.10.019.

[31] Sabio E, González E, González J F, et al. Thermal regeneration of activated carbon saturated with *p*-nitrophenol. Carbon, 2004, 42(11): 2285-2293. DOI: 10.1016/j.carbon.2004.05.007.

[32] Li T P, Sun T T, Li D X. Preparation, sintering behavior, and expansion performance of ceramsite filter media from dewatered sewage sludge, coal fly ash, and river sediment. Journal of Material Cycles and Waste Management, 2018, 20(1): 71-79. DOI: 10.1007/s10163-016-0547-3.

[33] Salvador F, Martin-Sanchez N, Sanchez-Hernandez R, et al. Regeneration of carbonaceous adsorbents. Part II: Chemical, microbiological and vacuum regeneration. Microporous and Mesoporous Materials, 2015, 202: 277-296. DOI: 10.1016/j.micromeso.2014.08.019.

[34] Román S, Ledesma B, González J F, et al. Two stage thermal regeneration of exhausted activated carbons. Steam gasification of effluents. Journal of Analytical and Applied Pyrolysis, 2013, 103: 201-206. DOI: 10.1016/j.jaap.2012.08.017.

[35] Li T P, Sun T T, Li D X. Removal of methylene blue from aqueous solution by ceramsite filter media combined with high temperature calcination for regeneration. Desalination and Water Treatment, 2016, 59: 220-229. DOI: 10.5004/dwt.2016.0239.

[36] Salvador F, Martin-Sanchez N, Sanchez-Montero M J, et al. Regeneration of activated carbons contaminated by phenol using supercritical water. The Journal of Supercritical Fluids, 2013, 74: 1-7. DOI: 10.1016/j.supflu.2012.11.025.

[37] Li T P, Sun T T, Aftab T B, et al. Adsorption isotherms, kinetics and thermodynamics of ammonium nitrogen from

aqueous solutions using modified ceramsite and its regeneration performance. Desalination and Water Treatment, 2017, 90: 196-205. DOI: 10.5004/dwt.2017.21239.

[38] Li T P, Sun T T, Aftab T B, et al. Photocatalytic degradation of methylene blue in aqueous solution using ceramsite coated with micro-Cu_2O under visible-light irradiation. Korean Journal of Chemical Engineering, 2017, 34(4): 1199-1207. DOI: 10.1007/s11814-017-0014-4.

[39] Miguel G S, Lambert S D, Graham N J D. The regeneration of field-spent granular-activated carbons. Water Research, 2001, 35(11): 2740-2748. DOI: 10.1016/S0043-1354(00)00549-2.

[40] Sharif F, Gagnon L R, Mulmi S, et al. Electrochemical regeneration of a reduced graphene oxide/magnetite composite adsorbent loaded with methylene blue. Water Research, 2017, 114: 237-245. DOI: 10.1016/j.watres.2017.02.042.

[41] Wang S Y, Tang Y K, Chen C, et al. Regeneration of magnetic biochar derived from eucalyptus leaf residue for lead(II) removal. Bioresource Technology, 2015, 186: 360-364. DOI: 10.1016/j.biortech.2015.03.139.

[42] Gamal M E, Mousa H A, El-Naas M H, et al. Bio-regeneration of activated carbon: A comprehensive review. Separation and Purification Technology, 2018, 197: 345-359. DOI: 10.1016/j.seppur.2018.01.015.

[43] Lin G, Cheng S, Wang S X, et al. Process optimization of spent catalyst regeneration under microwave and ultrasonic spray-assisted. Catalysis Today, 2018, 318: 191-198. DOI: 10.1016/j.cattod.2017.09.042.

[44] Zang T T, Cheng Z, Lu L, et al. Removal of Cr(VI) by modified and immobilized *Auricularia auricula* spent substrate in a fixed-bed column. Ecological Engineering, 2017, 99: 358-365. DOI: 10.1016/j.ecoleng.2016.11.070.